Quasi-periodic migration of single cells on short microlanes

Fang Zhou[1], Sophia A. Schaffer[1], Christoph Schreiber[1], Felix J. Segerer[1], Andriy Goychuk[2], Erwin Frey[2] and Joachim O. Rädler[1]*

[1] Faculty of Physics and Center for NanoScience, Ludwig-Maximilians-Universität München, Munich, Germany

[2] Arnold-Sommerfeld-Center for Theoretical Physics, Faculty of Physics and Center for NanoScience, Ludwig-Maximilians-Universität München, Munich, Germany

* Correspondence: Joachim O. Rädler

E-mail: raedler@lmu.de

Abstract

Cell migration on microlanes represents a suitable and simple platform for the exploration of the molecular mechanisms underlying cell cytoskeleton dynamics. Here, we report on the quasi-periodic movement of cells confined in stripe-shaped microlanes. We observe persistent polarized cell shapes and directed pole-to-pole motion within the microlanes. Cells depolarize at one end of a given microlane, followed by delayed repolarization towards the opposite end. We analyze cell motility via the spatial velocity distribution and frequency spectrum. The experimental data are compared to a Cellular Potts model that includes a minimal description of cytoskeleton dynamics. In particular, we evaluate the reversal time as a measure for spontaneous repolarization of cells as well as the time required to quench the leading lamellipodium at the microlane ends. Using LifeAct-GFP transfected cells and microlanes with differently shaped ends, we find distinct scenarios at the leading edge. Here, we show that the tip geometry and hence the local deformation of the leading edge of the cell has an effect on actin polymerization. Our experiments and computer simulations show that quasi-oscillatory cell motion on short lanes enables addressing how boundaries affect cytoskeleton advancement and repolarization dynamics in a repeated and quantitative manner.

Keywords: Cell migration, quasi-periodic, polarization, actin dynamic, micropattern

Introduction

Cells navigate in complex environments and undergo morphological changes via dynamic reorganization of the actin cytoskeleton [1, 2]. Movement is generated by cyclic phases of protrusion, adhesion to the extracellular environment, and actomyosin-driven retraction of the cell rear. Actin polymerization and crosslinking prevails in the advancement of filaments, protrusions and lamellipodia. Unraveling the mechanisms underlying actin transport, polymerization dynamics, and their regulation by Rho family GTPases are central challenges towards an intricate understanding of cell migration. The dynamics of actin indeed show many peculiarities, including traveling wave patterns [3-6], retrograde actin flow at the leading edge [2, 7-9], protrusion-retraction cycles as well as persistent polarity [5, 10]. In 2D cell culture, the actomyosin-driven shape changes of the cell body lead to phenotypic migratory modes that can be detected across large length scales. The macroscopically apparent persistent random walk is generated by the following key components: (i) persistence of leading protrusions and (ii) spontaneous front-rear polarization of cells. According to theory, cell polarization might emerge from a bi-stable reaction-diffusion system that is formed by intracellular signaling proteins [11]. Detailed spatiotemporal models of the signaling biochemistry of Rho family GTPases, which interact with the cell membrane and actin-binding proteins, were found to reproduce front-rear polarization and cell shape [12-15]. Apart from polarization, such bi-stable mass-conserving reaction-diffusion equations in general can also exhibit oscillations [16]. Here, related observations are the occurrence of actin waves or oscillatory cell shape dynamics. For example, in *Dictyostelium discoideum*, PIP signal polarization, as well as PI3K and PTEN regulation shows spontaneous waves and oscillations relevant for chemotaxis [17, 18]. However, even though these oscillations share general features, spontaneous large-scale oscillations in the eukaryotic cytoskeleton remain a rare phenomenon.

In recent years, artificial micropatterns have been used to confine cell migration to well-defined geometries [19], in particular microlanes [20-23]. On microlanes, cell motion is reduced to an effective 1D persistent random walk. There, a universal relation between persistence and cell velocity was shown to hold [7]. Other micropatterns with non-trivial geometries give rise to novel migratory behavior: circular adhesion islands lead to rotational migration of small cohorts of cells [24], ratchet geometries induce directed migration [25-27], cells confined in dumbbell-shaped micropatterns undergo repeated stochastic transitions characterized by intricate nonlinear migratory dynamics [28], and microlanes with gaps show

emergence of stochastic cell reversal and transits [29]. In addition, migration patterns may change upon interference with the cytoskeleton. For example, persistent cell migration on linear microlanes shifts to striking oscillations upon depolymerization of microtubules [30] or by depletion of zyxin, a protein that concentrates at focal adhesions and actin cytoskeleton components [31]. Because of their flexibility in controlling cell behavior, micropatterns are well suited to verify computational models of cytoskeleton dynamics and to advance our understanding of the underlying regulatory network. In particular, computer simulations have predicted periodic migration of cells on 1D micropatterns [32]. Similar findings were reported in reaction-diffusion models of actin waves on flexible and on circular boundaries [3, 33]. These theoretical studies suggest that confining geometries might reinforce sustained oscillations. However, systematic experimental studies of periodic cell migration on micropatterns have not yet been carried out. In particular, there have been no studies regarding the dynamics and curvature-dependence of repolarization in the presence of a boundary.

Here, we study the migration of single cells on short microlanes. Using micro contact printing, we create arrays of fibronectin-coated stripe-shaped micropatterns of different lengths. On these micropatterns, we observe quasi-periodic cell migration for the breast cancer cell line MDA-MB-231. We investigate how the spatial distribution of the cell position, the velocity distribution, and the periodicity of cell migration depend on the microlane length. Our data indicate that cells undergo repeated cycles of directed migration with pronounced cell polarization, followed by distinct termination of the cell's leading edge at the micropattern ends, and spontaneous cell repolarization in the opposite direction. We recapitulate these migratory features in a dynamic Cellular Potts model, which includes a simplified description of the adapting cell cytoskeleton [34]. Subsequently, we compare the distributions of apparent repolarization times between our experiments and computer simulations. Finally, we discuss how micropatterns constitute a controlled experimental framework that enables further investigation into the existence of excitable dynamics in actin-based cell migration.

Results and discussions

1. Single cell migration on stripe-shaped microlanes

In a first set of experiments, we investigated whether cells captured on microlanes exhibit oscillatory migration. Breast cancer cells (MDA-MB-231) are seeded on arrays of fibronectin-coated microlanes, which are surrounded by a PEGylated and therefore cell-repellent surface. These microlanes feature six different lengths between 70 and 270 µm. The fabrication of the

micropattern follows previous protocols and is described in detail in the methods section. Cells adhere, spread and remain confined within the microstructures during the entire period of the experiment. Movies were taken in time-lapse mode, recording images every 10 min over a period of 36 h. During this time, cells migrate in a guided manner and always align their front-rear polarity axis along the main axis of the microlanes. We observe repeated cycles of directed motion, termination of the motion at the micropattern ends, and cell repolarization in the opposite direction. This recurring sequence of events leads to quasi-periodic migration as shown in the time sequences in Fig 1a. Cells exhibit a typical migratory morphology with an actin-rich lamellipodium at the leading edge – seen as a dark rim in phase contrast – and a retracting tail at the rear. As cells reach the respective end of a microlane, they adopt a shortened, almost round appearance with no lamellipodium, until a newly formed lamellipodium appears at the opposite end of the cell body. These migratory and resting phenotypes coincide with distinct regimes of cell motion, which we obtain by tracking the cell nucleus. Fig 1b shows an exemplary trajectory of a cell nucleus over the course of 36 hours. The cell shows phases of directed motion followed by pausing and repolarization, thereby resulting in a quasi-periodic movement. Note that cell motion is quasi-periodic in the sense that the time needed for reorientation of the cell is stochastic, which leads to variability in the period of the back-and-forth motion.

Fig 1. Cell migration on microlanes: (a) Time sequence of a cell (MDA-MB-231) migrating on a stripe-shaped micropattern (Stripe length L = 120 µm, width W = 20 µm, 10 min time intervals). Images are taken in phase contrast and with fluorescence microscopy. The nucleus is labeled with Hoechst 3334 as indicated in blue. (b) Trajectory of cell nucleus tracked over the course of 36 h showing quasi-periodic alternations between directed migration and repolarization.

2. Spatial velocity distribution

In order to better distinguish phases of directed migration from phases of reorientation, we fabricated microlanes of different lengths. A sufficiently large sample size of hundreds of cells was acquired by parallel automated tracking of fluorescently labeled cell nuclei. Our automated image analysis yields cell trajectories $x(t)$ as described in the Materials and Methods. The instantaneous cell velocities are determined by $v(t) = [x(t + \Delta t) - x(t)]/\Delta t$, where $\Delta t = 10\,min$ is the time interval between two subsequent frames. Fig 2 shows exemplary single cell trajectories together with the spatial distributions of cell positions and velocities, which were sampled from ensembles of about 100 cells for each microlane length. These distributions are determined by binning the cell positions into 5 µm sections along the microlane, and then computing the fraction $p(x)$ and the mean absolute velocity $\langle|v|\rangle(x)$ of

cells found in each bin. Cells on the shortest microlane (L = 70 µm) do not exhibit periodic motion, and instead remain in a symmetric morphology with two lamellipodia extending at the cell tips. Evidently, there is not enough space for directional migration on short microlanes. In contrast, quasi-periodic migration is observed on longer microlanes (L = 120 - 270µm). Fig 2b shows that the detection frequency of cell nuclei decreases towards the micropattern tips and becomes flat in the middle of the microlanes. Similarly, the mean absolute velocity distributions decline towards the micropattern tips and show a distinct plateau behavior at the case of longer microlanes (220 µm and 270 µm), with mean absolute velocities ranging from 0.3 - 0.6 µm/min (Fig 2c).

Fig 2. Migration pattern as a function of lane length: From left to right: (a) Time courses of cell nucleus position of cells within microlanes. (b) Spatial distributions of nuclei. (c) Spatial distributions of mean absolute cell velocity. Blue lines are SE for the binned data. (d) Schematic drawing of the microlanes with length L = 70, 120, 170, 220, 270 µm and width W = 20 µm. Dashed lines indicate the transition between microlane tips and microlane center. These results were obtained by binning the cell positions (5µm bin width). For each micro-pattern stripe length, we tracked roughly 100 cells.

Cell speeds are uniformly distributed in the center of the microlanes and decline at the tips, where cell repolarization occurs. In order to differentiate these two microlane regions, we look more closely at the mean absolute velocity distribution. The spatial velocity distributions appear to have a trapezoidal profile, where two velocity ramps at the microlane tips are connected by a plateau in the microlane center. Then, we determine the transition points between the ramp (repolarization) and plateau (run) regions (see black dashed lines in Fig 2). In order to identify these transition points, we apply a change-point-analysis as described in the Supporting Information S2. We find that the distance from the transition points to the tip of the microlane $\xi_0 = 55\ \mu m$ is nearly constant across all micropattern lengths. Thus, cells on 120 µm stripes are able to polarize but have only a very short migration phase until interacting with the opposite boundary. In the center of longer microlanes (L =170, 220, and 270 µm), we find longer phases of directed motion in which cells migrate with a mean absolute velocity of approximately 0.4 - 0.6 µm/min.

3. Velocity distribution and sustained oscillations

We further quantify the quasi-periodic migration of cells. First, we determine the overall distribution of absolute cell velocities (Fig 3a). We find that for microlanes long enough to show persistent cell migration (L=120-270µm), the cell velocity distributions collapse onto an exponentially decaying master curve. Short microlanes, where we do not observe persistent cell migration, show a distinctly narrower velocity distribution. This is likely explained by the

observation that cell repolarization begins at a distance of 55µm from the micropattern tips. If the microlane is shorter than this distance, then the cell is in a constant state of repolarization, which diminishes oscillatory motion.

Fig 3. Overall spectral analysis of the large ensemble of cell traces. (a) Normalized distribution of absolute cell velocities, $\langle|v|\rangle$, for single MDA-MB-231 cells migrating in stripe-shaped micro patterns of five different lengths and fixed width (W=20 µm). Inset: Non-normalized (counts) velocity distribution in a logarithmic plot. (b) Discrete Fourier transform of the time-dependent directional velocities, fitted by a log-normal distribution (lines). (c) The migration period (T=1/frequency) of single cells increases linearly with the stripe length. The error bars correspond to the peak width of the fitting in (b).

Subsequently, we performed a discrete Fourier transform of the cell velocity time-traces for different stripe lengths, which yields the frequency distribution corresponding to the quasi-periodic cell migration. We find that the frequency spectrum follows a log-normal distribution. Furthermore, the dominant frequency (f_{max}, peak of the frequency spectrum) shifts to lower frequencies for longer stripe lengths. This indicates that cells move with a constant velocity across the micro-lane. To demonstrate this hypothesis, we plot the period of migration, $T = 1/f_{max}$, against the stripe length (Fig 3c). We find that the period of migration increases linearly with the stripe length, at a slope $dT/dL = 0.054 \pm 0.006$ h/µm. This corresponds to a constant average velocity of pole-to-pole migration, $v_c = 0.62\ \mu m/min$, which is in good agreement with the velocity plateau in the stripe centers (Fig 2).

4. Repolarization time

In the following, we address cell repolarization and the dynamics of directed migration reversal at the ends of the microlanes. We observe that cells depolarize when the protruding lamellipodium encounters the confining PEG-layer. The cell then compacts as its trailing edge continues to move. As the trailing edge stalls, the cell begins to expand again and finally repolarizes towards the opposite, free cell edge. This repolarization manifests itself in a new lamellipodium that emerges at the free cell edge. Note that this phenomenon of internal repolarization is rather specific for cells confined on tracks. The more general appearance of mesenchymal cell migration in 2D as well as 3D appears to redirect existing lamellipodia or exhibit several competing lamellipodia. However, in the experiments presented here, the appearance of lamellipodia is restricted to two sides of the cell due to its lateral confinement by the microlanes. Hence, reorientation of crawling cells occurs via a relatively well-defined cycle of depolarization and repolarization. This feature allows us to examine the "reversal time", which is a measure for the time scale of depolarization and repolarization when a cell reaches the end of a microlane. To this end, we define a reversal area A_0 at the ends of the

stripes (Fig 4a) that marks the regions where the velocities are observed to decrease in Figure 2(with a distance ξ_0 = 55 µm to the boundary). During a depolarization-repolarization cycle, a cell first enters the reversal area at $t = t_1$ when it approaches the microlane tip, and leaves it at $t = t_2$ after repolarization. Therefore, we define the reversal time as $t_R = t_2 - t_1$ and determine its distribution for four different micro-lane lengths (Fig 4b). We note that the distributions are independent of the stripe length. Although the exact value of the average reversal time will typically depend on the particular choice of the reversal area, we consistently find an average depolarization and repolarization time of approximately 100 min.

Fig 4. Distribution of "reversal times": (a) Schematic drawing of a cell entering the microlane tip region A_0, arresting and then returning from the tip region, with the leading edge of the cell shaded in dark green. The red dashed line indicates the position of cell entry into the tip region A_0, at time t_1, and exit of the tip region, at time t_2. (b) The normalized distribution of the reversal times $t_R = t_2 - t_1$ for four different microlane lengths. Inset: Non-normalized (counts) distribution of the reveral times.

5. Cellular Potts model recapitulates quasi-periodic motion

The data presented so far are obtained from a large cell ensemble. Therefore, the distribution functions that describe the quasi-oscillatory cell motion present a robust and generic testbed for comparison with mathematical modeling. Recently, we have developed an extended Cellular Potts model that is capable of describing spatiotemporal dynamics of cells in 2D [24, 34]. In particular, we model the spatiotemporal dynamics of the contact area of a cell with a planar substrate, which is described by a set of discrete adhesion sites on a 2D lattice. In addition to a simplified description of the mechanical properties of cells [35-37], we also account for a minimal mechanism of cell polarization. Specifically, we include an internal self-regulating *polarization field* within each individual cell, which emulates effective protrusive forces due to actin polymerization, as well as actomyosin contractility and cell-substrate adhesions. This polarization field is regulated via intracellular signals that are assumed to have a fixed range. In more detail, we simplify all intracellular signaling, which is mediated e.g. by the Rho GTPase family of proteins, into two prototypical feedback loops: (i) cell protrusions reinforce the protrusion field and lead to further protrusions and (ii) cell retractions weaken the protrusion field and lead to further retractions [24, 34].

We then simulated individual cells with fixed parameters and constant average area on stripe-shaped microlanes. Note that this premise already marks a striking difference from the experiments: in the simulations we investigate a population of clonal and therefore identical cells, while the cells used in the experiments show a wide variation in morphology and

migratory behavior. Therefore, we expect the simulations to underestimate all variances compared to the experiments. Furthermore, we adjusted the duration of a Monte Carlo step so that the average absolute velocity of migrating simulated cells, $\langle |v| \rangle = 0.6\ \mu m/min$, matches the experiments. Based on our previous work[34, 38], we modified the parameters to account for cell persistence and stochasticity, and to achieve a sufficiently fine discretization of the cell body to resolve the micropattern tips. A detailed description of the parameters is provided in the Supporting Information S1.

With the simulated cell trajectories being in good agreement with experimental data (Fig 5), we find that the model reproduces the quasi-oscillatory motion observed in our experiments. We then evaluated the distribution of cell reversal times in the simulations analogously to the experiments, observing a pronounced peak at 100 min (Fig 5c). Furthermore, the simulated cells show a similar spatial velocity distribution as in the experiments (Fig 5d). In addition, we also performed more intuitive comparisons between simulations and experiments. In particular, we find similar morphologies of (i) polarized and persistently migrating cells with a flat leading edge and a tapered rear, (ii) cells that depolarize after running into a dead end on the microlane, and (iii) repolarized cells (Fig 5a). In addition, to assess actin distribution during cell migration, we transfected live cells with a fusion construct of the actin-binding peptide LifeAct and GFP (LifeAct-GFP). Intuitively comparing the representative kymographs for both a simulated cell and an experimental LifeAct-GFP transfected cell, both demonstrate similar oscillations on the same microlane (Fig 5b). Our findings suggest that the quasi-periodic migration of cells on microlanes is well described by an extended Cellular Potts model. This model predicts emergent cell polarization from stochastic occurrence and self-reinforcement of cell protrusions, which then leads to a stochastic (re)polarization time. However, we also note a qualitative difference between experiments and simulations. It seems likely that there is a sharper actin accumulation at the leading edge in experiments, in contrast to the polarization field (which can be seen as a proxy for the cytoskeleton density) of a simulated cell decreasing progressively from front to rear.

Fig 5. Comparison of computer simulation and experimental results. The microlane length is fixed at 150 µm with a round tip geometry. (a) The extended Cellular Potts model features an internal polarization field. the simulation reproduces the distinct run and rest phenotypes and yields cell center-of-mass trajectories that show quasi-periodic behavior (bottom); experimentally obtained cell trajectories are indicate on the upper right. (b) Comparison between the kymograph of a LifeAct-GFP transfected MDA-MB-231 cell with nuclear staining (bottom) and the kymograph of a simulated cell. Top: Zoom-in into a region that contains two periods of oscillation. Top left: Simulated cell. Top right: Experimental cell. Bottom: Zoom-out to the kymograph of an

experimental cell that performs many periods of oscillation. Red arrows indicate actin dynamics in the front of the cells. (c) Reversal time distributions of simulated and experimental cells. (d) Spatial mean absolute velocity distribtuions of simulated and experimental cells.

6. Effect of curvature on cell depolarization

It is understood that the non-linear dynamics of actin polymerization and turnover depends on the cell shape and the geometry in which the cell migrates [14, 39]. In order to test the interplay between surface geometry and cell contour, we investigate the depolarization and repolarization of cells on microlanes with differently shaped tips. For example, a tapered tip allows us to explore how the reversal time depends on the deformation of the leading lamellipodium. To this end, we fabricated microlanes with four distinctly curved tips: round-, blunt-, sharp-, and concave-shaped, while keeping the total area and the width of the stripes constant (Fig 6a) to assure the comparability of the cell behavior. In order to observe many reversal events but also directed migration we established a length of 170 μm for the round tips. Thus, depending on the tip geometry the length of the stripes is slightly different to achieve a constant area. Exemplary fluorescent images of the adhesion micro-patterns are shown in Fig 6b. Across all studied geometries, we find that cells consistently exhibit oscillatory motion. Furthermore, the distribution of reversal times, or in other words, the depolarization-repolarization time, does not depend significantly on the respective tip geometry (Fig 6c). All reversal times are centered around approximately 100 min, which is consistent with the results in Fig. 4b. Evidently, tip curvature does not play a significant role in determining the reversal time for a defined tip area. A comparison between experiments and simulations, using the same algorithms for the analysis, yields similar reversal times (Fig 6d). However, the reversal time distribution is typically broader in the experiments than in the simulations, indicating that our simulations might underestimate the cell variability. Note, that it is equally likely that the broad distribution of reversal times in the experiments originates from cell-to-cell variability in the ensemble, e.g. cell size, which is not considered by the simulations at all.

Fig 6. Effect of curvature on the repolarization time. (a) Schematic diagram of micropattern geometry with four different tip shapes: blunt, concave, round, and sharp. The area of all stripes and the reversal area A_0 are kept constant same. (b) Exemplary fluorescent images of microlanes of width W=20 μm. (c, d) The distribution of cell reversal times (Δt) when reaching the microlane tips, for four different tip shapes. The cell enters the reversal area A_0 from the corresponding microlane tip. (c) Experimental reversal time distribution. (d) Simulated reversal time distribution.

To gain additional insight into the spatiotemporal actin dynamics at the leading edge of the cell, we recorded a series of live time-lapse images of LifeAct-GFP transfected MDA-MB-231 cells. LifeAct, which is an actin-binding peptide-GFP fusion construct, does not interfere with actin dynamics [40]. The deformation of the leading edge and the spatial distribution of F-actin in the protrusions are visualized in a close-up image series of the advancing lamellipodium at the microlane ends (Fig 7). There, we also show snapshots of the leading edge of simulated cells for a direct comparison between experiment and simulation. Both in experiments and simulations, we find that the lamellipodium splits in the concave-shaped end and is focused in a sharp tip. These findings indicate that the local actin assembly is determined by the local curvature of the confining PEG-border. Furthermore, our experiments show that the cell contour is not entirely adjusted to the contour of the fibronectin/PEG interface. In many instances, we find transient actin protrusions into the PEGylated area. Because the PEGylated area does not constitute a solid mechanical boundary in our experiments, actin protrusions may invade into this region. However, the cell is not capable of adhering to the underlying substrate, leading to a subsequent retraction. In contrast, in our computer simulations we strictly confine the cell contour to the micropattern. Furthermore, in the simulation, the contour of the advancing cell edge does not adopt the shape of the concave and sharp microlane tips to the same degree as in the experiments (Fig 7c and d). This might be due to (i) an overestimation of the perimeter stiffness or (ii) prohibiting the simulated cell from leaving the micropattern, which would allow less curved cell shapes.

Figure 7: Geometry dependence of migratory arrest: Comparison between LifeAct GFP labeled MDA-MB-231 cells and simulated cells, which migrate towards differently shaped micro-lane tips (Lane length L=170 μm, width W=20 μm). The top row (in green) shows fluorescence time-lapse data, while the bottom row shows the corresponding computer simulation for a) round-shaped tips b) blunt-shaped tips c) sharp-shaped tips and d) concave-shaped tips.

Conclusion

In this work, we investigate single cells that migrate within a confinement in the form of short microlanes. The dominant oscillation frequency, the spatial distribution of cell positions and the persistent velocity of polarized migrating cells as a function of microlane length confirm a pole-to-pole migration mode. We find that cells migrate in a stochastic, quasi oscillatory manner with repetitive depolarization-repolarization processes. A morphological view of this quasi-periodic migration highlights the repetitive depolarization and repolarization of cells. At the poles of the microlanes, cell polarization and hence cell advancement is quenched due

to contact with the PEGylated area. Then, spontaneous protrusions of the cell along its opposite, free edge and subsequent polarization in the opposite direction reverses the cell motion. The reversal time does neither depend on the length nor on the geometry of the microlane ends. We find that the experimentally observed pole-to-pole cell migration mode is recapitulated by an extended Cellular Potts model. Our model shows that the distribution of stochastic repolarization times might be explained as follows: stochastic membrane protrusions explore the vicinity of the cell. Then, if the cell can adhere in the explored region, these protrusions form stable lamellipodia through a self-reinforcing feedback loop. In addition, the model also captures details of the spatiotemporal evolution of the actin polymerization front, such as lamellipodium splitting in concave tip geometries. These findings are surprising, since, the Cellular Potts model does not currently take into account any molecular details of the cytoskeleton. Further development of the Cellular Potts model to include myosin and the actin regulating Rho GTPases, which has been the subject of interest in analytical reaction-diffusion models of moving cells [7, 11-14], will possibly improve predictions of the morphology and dynamics of the moving cell. In this context, the microlane assay proves useful as a testbed for future theory, facilitating the accumulation of statistics over repeated de- and repolarization events. As a cell depolarizes in different microlane geometries, the resulting spatial distribution of actin activity could lead to a better understanding of how cell adhesion and the local membrane curvature regulate actin polymerization [18, 39, 41, 42]. In particular, computational models are challenged to recapitulate migratory behavior on various micro-pattern geometries in a consistent manner using an optimized, unique parameter set. Here, future studies combining cell migration assays on micropatterns and computational models will be valuable for classifying cytoskeleton dynamics and mechanisms that lead to distinct migration phenotypes in confinement.

Materials and methods

Micropatterning.

Laser lithography. To prepare the master mold of the stamp for micropatterning, a silicon wafer was coated with TI Prime adhesion promoter and AZ40XT (MicroChemicals) photoresist. Areas for cell adhesion were exposed to UV light using laser direct imaging (Protolaser LDI, LPKF). The photoresist was developed (AZ 826 MIF, MicroChemicals) and then silanized (Trichloro(1H,1H,2H,2H-perfluorooctyl)silane, Sigma-Aldrich). To fabricate the stamp, polydimethylsiloxane (PDMS) monomer and crosslinker (DC 184 elastomer Kit,

Dow Corning) were mixed in a 10:1 ratio (w/w), poured onto the master mold, and cured 3 h or overnight at 50°C. The crosslinked PDMS layer was peeled off and manually cut into stamps.

Microcontact printing: Stripe-shaped microlanes were produced by microcontact printing. Firstly, PDMS stamps were exposed with UV-light (PSD-UV, Novascan Technologies) for 5 min. The stamps were then immersed in an aqueous solution of 40 µg/ml fibronectin (Yo Proteins) containing 10 µg/ml Alexa Fluor 488 dye (Life Technologies) labeled fibronectin for 45 min. The stamps were subsequently washed with ultrapure water. Stamps were dried under filtered airflow and then stamped onto a hydrophobic uncoated µ-Dish (Ibidi GmbH) bottom that underwent UV exposure for 15 min beforehand. The stamps were gently pressed with tweezers for a few seconds to ensure contact with the bottom. To then fabricate the cell-repelling areas, 30 µL of 2 mg/ml poly-L-lysine-grafted polyethylene glycol (PLL-g-PEG) (2 kDa PEG chains, SuSoS) dissolved in 10 mM Hepes and 150 mM NaCl solution was added. After the removal of the stamps, a glass cover slip was placed on the printed bottom to assure complete coverage with the PEG solution and then incubated for 30 min at room temperature. Finally, the printed bottom was washed with phosphate buffered saline (1xPBS) three times and stored in 1x PBS for further cell seeding. Unless otherwise specified, the patterns consisted of uniform stripes 20 µm in width.

Cell culture and transfection.

MDA-MB-231 breast cancer cells were cultured in modified Eagle´s medium (MEM-F10, c.c.pro) supplemented with 10% fetal calf serum (FCS, Invitrogen) and 2.5 mM L-glutamin (c.c.pro) at 37°C in 5% CO2 atmosphere. For time-lapse phase-contrast images, cells were seeded at a density of 1 x 10^4 cells per dish (µ-Dish, IBIDI). After 2 h, cell medium was replaced by 1 ml Leibovitz's L-15 Medium (c.c.pro) containing 10% FCS and 25 nM Hoechst 33342 nucleic acid stain (Invitrogen) and incubated for 1 h at 37°C before imaging.

For actin dynamics studies, seeded cells were further transfected with LifeAct-GFP mRNA. Briefly, ~1x 10^4 cells were seeded into a 35mm µ-Dish and incubated 2 h at 37°C in 5% CO2 for cell adhesion. 1.25 µl Lipofectamine MessengerMax Reagent (Invitrogen) was diluted in 123.75µl OptiMEM (Life Technologies) transfection medium and incubated 10 min at room temperature. 500 ng mRNA (0.5 µl x 1000 ng/µl) was diluted in 124.5 µl OptiMEM. Both solution were mixed and incubated for 5 min at room temperature for lipoplex formation. Adhered cells were washed with 1xPBS, and carefully added to the 250 µl transfection mix. After a 1 h incubation at 37°C in 5% CO2, the cell transfection mix was replaced by 1 ml

Leibovitz's L-15 Medium (c.c.pro) containing 10% FCS before proceeding to time lapse imaging.

Live cell imaging and microscopy.

For migration studies, scanning time lapse measurements were acquired using an automated inverted microscope iMIC (Till Photonics). The microscope was equipped with a 10x Zeiss objective and a 40x Zeiss objective, an ORCA-03G camera (HAMAMATSU), and an Oligochrome lamp (Till Photonics). During the measurements, cells were maintained in L-15 Meidium containing 10% FCS at 37°C using a temperature-controlled mounting frame (Ibidi temperature controller, Ibidi). Phase contrast and fluorescent images were automatically acquired at 10 min intervals, unless noted otherwise. To analyze the actin dynamics at the interface of micropatterns, images were acquired at intervals between 20 s - 1 min.

Image processing and data analysis.

Image analysis was carried out using ImageJ (National Institutes of Health, NIH). Images of isolated cells migrating in the stripe-shaped microlanes were first manually cropped. The trajectory of each stained nucleus was preprocessed by first applying a bandpass filter and a threshold to the fluorescence images, and the geometric center of mass of the nucleus was subsequently evaluated. The geometric mean of the nucleus position was used as a proxy for the cell position. Only cells that explored the whole stipe where analysed. Cell tacks were excluded from further analysis in the following cases: cell tracks shorter than 36 h, cell division or spanning out of the micropattern, and tracks of non-moving or dead cells.

Trajectories of individual cells were analyzed in Matlab. Therefore, only the component in direction of the microlane was considered resulting in a 1D trajectory. The center of the microlane was determined by taking the middle of the two points where cells got closest to each tip of the microlane.

Acknowledgements

This work was supported by grants from the Deutsche Forschungsgemeinschaft (DFG) via the Collaborative Research Center (SFB) 1032 (Project B01 and B02) and the excellence cluster NanoSystems Initiative Munich (NIM). F.Z. acknowledges support by the China Scholarship Council (CSC).

References

1. Mitchison TJ, Cramer LP. Actin-Based Cell Motility and Cell Locomotion. Cell. 1996;84(3):371-9.
2. Keren K, Pincus Z, Allen GM, Barnhart EL, Marriott G, Mogilner A, et al. Mechanism of shape determination in motile cells. Nature. 2008;453(7194):475-80.
3. Kruse K, Camalet S, Julicher F. Self-propagating patterns in active filament bundles. Phys Rev Lett. 2001;87(13).
4. Carlsson AE. Dendritic Actin Filament Nucleation Causes Traveling Waves and Patches. Phys Rev Lett. 2010;104(22):228102.
5. Giannone G, Dubin-Thaler BJ, Dobereiner HG, Kieffer N, Bresnick AR, Sheetz MP. Periodic lamellipodial contractions correlate with rearward actin waves. Cell. 2004;116(3):431-43.
6. Bretschneider T, Anderson K, Ecke M, Müller-Taubenberger A, Schroth-Diez B, Ishikawa-Ankerhold HC, et al. The Three-Dimensional Dynamics of Actin Waves, a Model of Cytoskeletal Self-Organization. Biophysical Journal. 2009;96(7):2888-900.
7. Maiuri P, Rupprecht J-F, Wieser S, Ruprecht V, Bénichou O, Carpi N, et al. Actin Flows Mediate a Universal Coupling between Cell Speed and Cell Persistence. Cell. 2015;161(2):374-86.
8. Shao D, Levine H, Rappel W-J. Coupling actin flow, adhesion, and morphology in a computational cell motility model. Proceedings of the National Academy of Sciences. 2012;109(18):6851-6.
9. Allard J, Mogilner A. Traveling waves in actin dynamics and cell motility. Current Opinion in Cell Biology. 2013;25(1):107-15.
10. Verkhovsky AB. The mechanisms of spatial and temporal patterning of cell-edge dynamics. Curr Opin Cell Biol. 2015;36:113-21.
11. Mori Y, Jilkine A, Edelstein-Keshet L. Wave-Pinning and Cell Polarity from a Bistable Reaction-Diffusion System. Biophysical Journal. 2008;94(9):3684-97.
12. Edelstein-Keshet L, Holmes WR, Zajac M, Dutot M. From simple to detailed models for cell polarization. Philosophical Transactions of the Royal Society B: Biological Sciences. 2013;368(1629).
13. Byrne Kate M, Monsefi N, Dawson John C, Degasperi A, Bukowski-Wills J-C, Volinsky N, et al. Bistability in the Rac1, PAK, and RhoA Signaling Network Drives Actin Cytoskeleton Dynamics and Cell Motility Switches. Cell Systems. 2016;2(1):38-48.

14. Marée AFM, Grieneisen VA, Edelstein-Keshet L. How Cells Integrate Complex Stimuli: The Effect of Feedback from Phosphoinositides and Cell Shape on Cell Polarization and Motility. PLOS Computational Biology. 2012;8(3):e1002402.
15. Falcke M. Concentration profiles of actin-binding molecules in lamellipodia. Physica D: Nonlinear Phenomena. 2016;318-319:50-7.
16. Halatek J, Frey E. Rethinking pattern formation in reaction–diffusion systems. Nature Physics. 2018;14(5):507-14.
17. Hoeller O, Toettcher JE, Cai H, Sun Y, Huang C-H, Freyre M, et al. Gβ Regulates Coupling between Actin Oscillators for Cell Polarity and Directional Migration. PLOS Biology. 2016;14(2):e1002381.
18. Hsu H-F, Bodenschatz E, Westendorf C, Gholami A, Pumir A, Tarantola M, et al. Variability and Order in Cytoskeletal Dynamics of Motile Amoeboid Cells. Phys Rev Lett. 2017;119(14):148101.
19. Lautenschläger F, Piel M. Microfabricated devices for cell biology: all for one and one for all. Current opinion in cell biology. 2013;25(1):116-24.
20. Maiuri P, Terriac E, Paul-Gilloteaux P, Vignaud T, McNally K, Onuffer J, et al. The first World Cell Race. Current Biology. 2012;22(17):R673-R5.
21. Wilson K, Lewalle A, Fritzsche M, Thorogate R, Duke T, Charras G. Mechanisms of leading edge protrusion in interstitial migration. Nature Communications. 2013;4:2896.
22. Doyle AD, Wang FW, Matsumoto K, Yamada KM. One-dimensional topography underlies three-dimensional fibrillar cell migration. The Journal of cell biology. 2009;184(4):481-90.
23. Picone R, Ren X, Ivanovitch KD, Clarke JDW, McKendry RA, Baum B. A Polarised Population of Dynamic Microtubules Mediates Homeostatic Length Control in Animal Cells. PLOS Biology. 2010;8(11):e1000542.
24. Segerer FJ, Thüroff F, Piera Alberola A, Frey E, Rädler JO. Emergence and Persistence of Collective Cell Migration on Small Circular Micropatterns. Phys Rev Lett. 2015;114(22):228102.
25. Mahmud G, Campbell CJ, Bishop KJM, Komarova YA, Chaga O, Soh S, et al. Directing cell motions on micropatterned ratchets. Nature Physics. 2009;5:606.
26. Caballero D, Voituriez R, Riveline D. The cell ratchet: Interplay between efficient protrusions and adhesion determines cell motion. Cell Adhesion & Migration. 2015;9(5):327-34.
27. Caballero D, Comelles J, Piel M, Voituriez R, Riveline D. Ratchetaxis: Long-Range Directed Cell Migration by Local Cues. Trends in Cell Biology. 2015;25(12):815-27.

28. Brückner DB, Fink A, Schreiber C, Röttgermann PJF, Rädler JO, Broedersz CP. Publisher Correction: Stochastic nonlinear dynamics of confined cell migration in two-state systems. Nature Physics. 2019;15(6):617-.
29. Schreiber C, Segerer FJ, Wagner E, Roidl A, Rädler JO. Ring-Shaped Microlanes and Chemical Barriers as a Platform for Probing Single-Cell Migration. Scientific Reports. 2016;6:26858.
30. Zhang J, Guo WH, Wang YL. Microtubules stabilize cell polarity by localizing rear signals. Proceedings of the National Academy of Sciences of the United States of America. 2014;111(46):16383-8.
31. Fraley SI, Feng Y, Giri A, Longmore GD, Wirtz D. Dimensional and temporal controls of three-dimensional cell migration by zyxin and binding partners. Nat Commun. 2012;3:719.
32. Camley BA, Zhao Y, Li B, Levine H, Rappel W-J. Periodic Migration in a Physical Model of Cells on Micropatterns. Phys Rev Lett. 2013;111(15).
33. Mogilner A, Keren K. The Shape of Motile Cells. Current Biology. 2009;19(17):R762-R71.
34. Thueroff F, Goychuk A, Reiter M, Frey E. Bridging the gap between single cell migration and collective dynamics. bioRxiv. 2019:548677.
35. Daub JT, Merks RMH. A Cell-Based Model of Extracellular-Matrix-Guided Endothelial Cell Migration During Angiogenesis. Bulletin of Mathematical Biology. 2013;75(8):1377-99.
36. Kabla AJ. Collective cell migration: leadership, invasion and segregation. Journal of The Royal Society Interface. 2012;9(77):3268-78.
37. Merks RMH, Glazier JA. A cell-centered approach to developmental biology. Physica A: Statistical Mechanics and its Applications. 2005;352(1):113-30.
38. Segerer FJ, Thüroff F, Alberola AP, Frey E, Rädler JO. Emergence and persistence of collective cell migration on small circular micropatterns. Phys Rev Lett. 2015;114(22):228102.
39. James J, Goluch ED, Hu H, Liu C, Mrksich M. Subcellular curvature at the perimeter of micropatterned cells influences lamellipodial distribution and cell polarity. Cell motility and the cytoskeleton. 2008;65(11):841-52.
40. Riedl J, Crevenna AH, Kessenbrock K, Yu JH, Neukirchen D, Bista M, et al. Lifeact: a versatile marker to visualize F-actin. Nature Methods. 2008;5:605.
41. Jeon H, Koo S, Reese WM, Loskill P, Grigoropoulos CP, Healy KE. Directing cell migration and organization via nanocrater-patterned cell-repellent interfaces. Nature materials. 2015;14(9):918.

42. Jiang X, Bruzewicz DA, Wong AP, Piel M, Whitesides GM. Directing cell migration with asymmetric micropatterns. Proceedings of the National Academy of Sciences. 2005;102(4):975-8.

Supporting information

Table S1. Parameters used for the computational simulation in this work.

Table S2. Number of analyzed cells for different lengths of microlane with round tips.

Table S3. Number of analyzed cells for of microlanes with different geometric tips.

Fig. S1 Mean cell velocity as a function of the distance to the nearest tip in microlanes of different lengths.

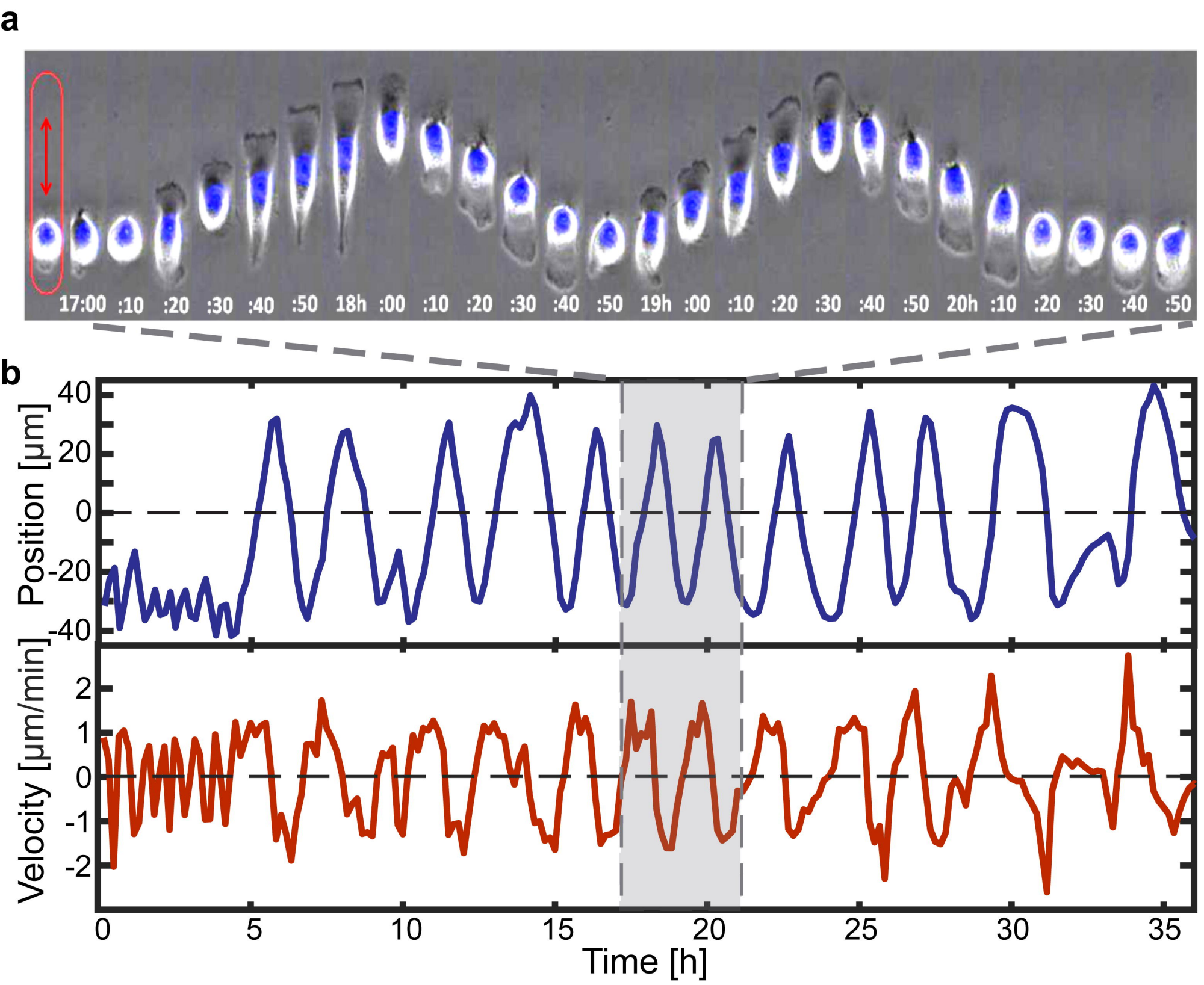
a
17:00
:10
:20
:30
:40
:50
18h
:00
:10
:20
:30
:40
:50
19h
:00
:10
:20
:30
:40
:50
20h
:10
:20
:30
:40
:50
b
Position [µm]
40
20
0
-20
-40
Velocity [µm/min]
2
1
0
-1
-2
0
5
10
15
20
25
30
35
Time [h]

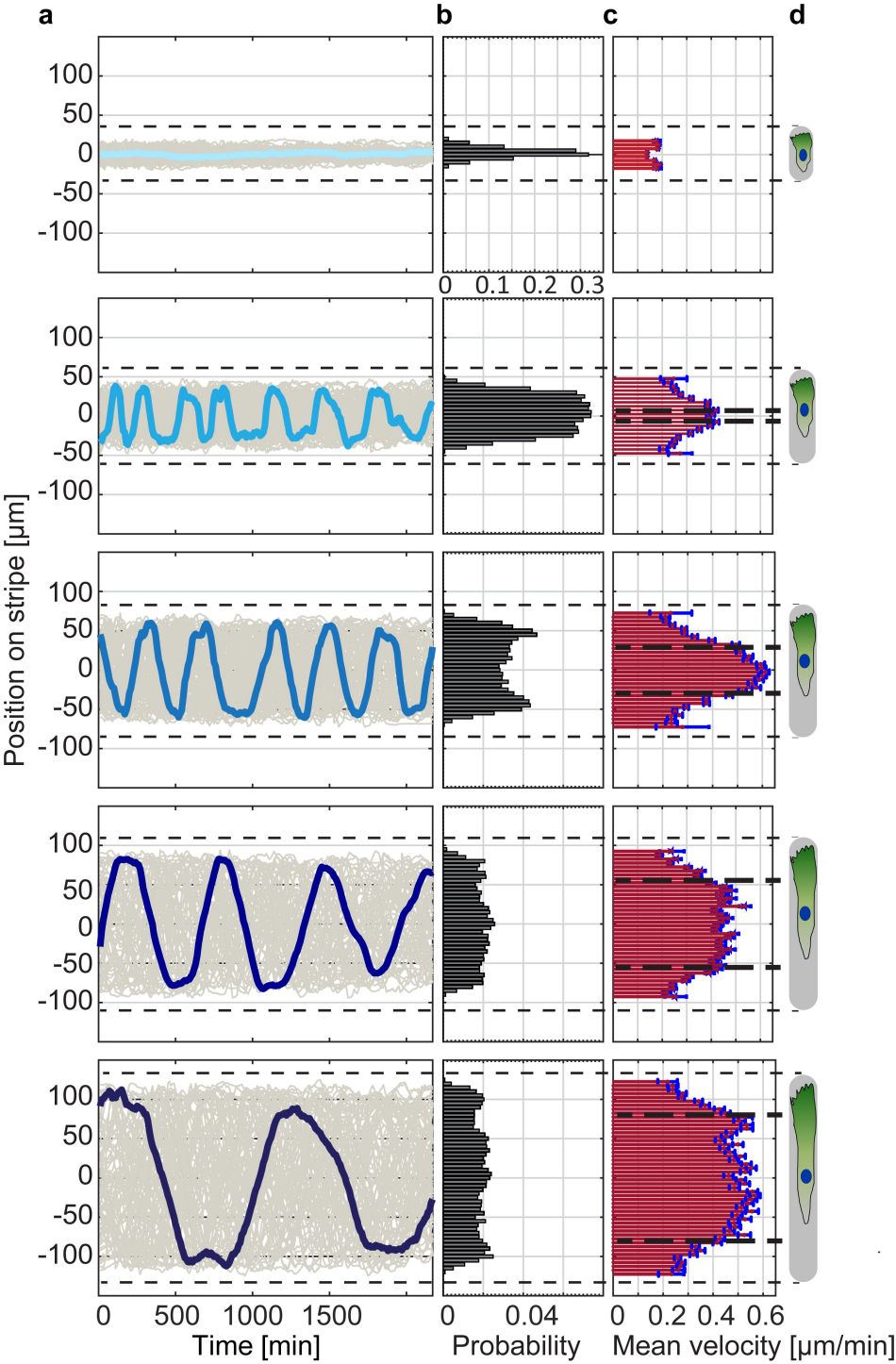
a
b
c
d
100
50
0
-50
-100
0 0.1 0.2 0.3
Position on stripe [µm]
0 500 1000 1500
Time [min]
0 0.04
Probability
0 0.2 0.4 0.6
Mean velocity [µm/min]

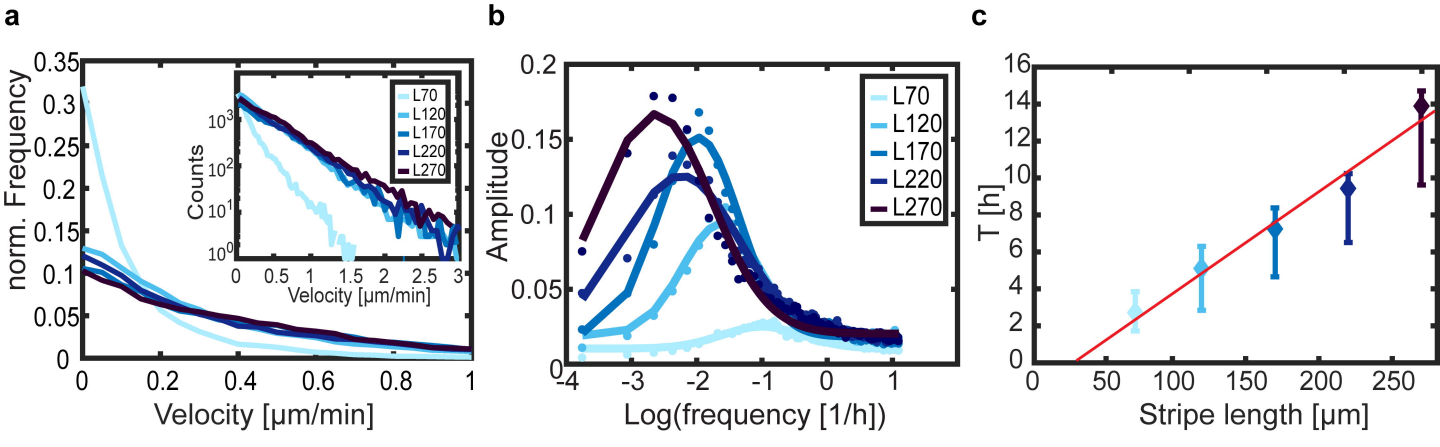
a
b
c
norm. Frequency
Velocity [µm/min]
Counts
Velocity [µm/min]
L70
L120
L170
L220
L270
Amplitude
Log(frequency [1/h])
T [h]
Stripe length [µm]

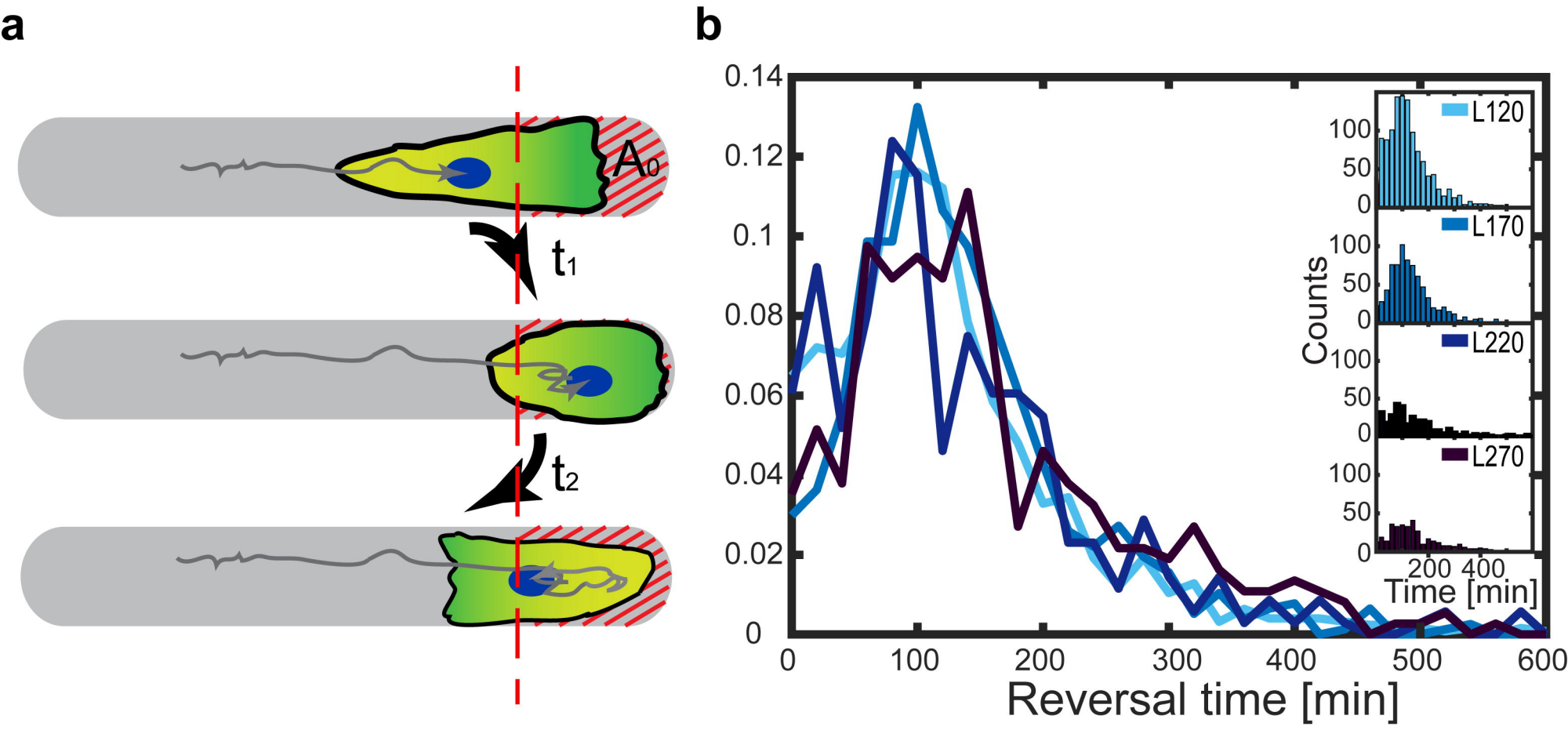
a
A_0
t_1
t_2
b
0.14
0.12
0.1
0.08
0.06
0.04
0.02
0
0
100
200
300
400
500
600
Reversal time [min]
Counts
L120
L170
L220
L270
100
50
0
200 400
Time [min]

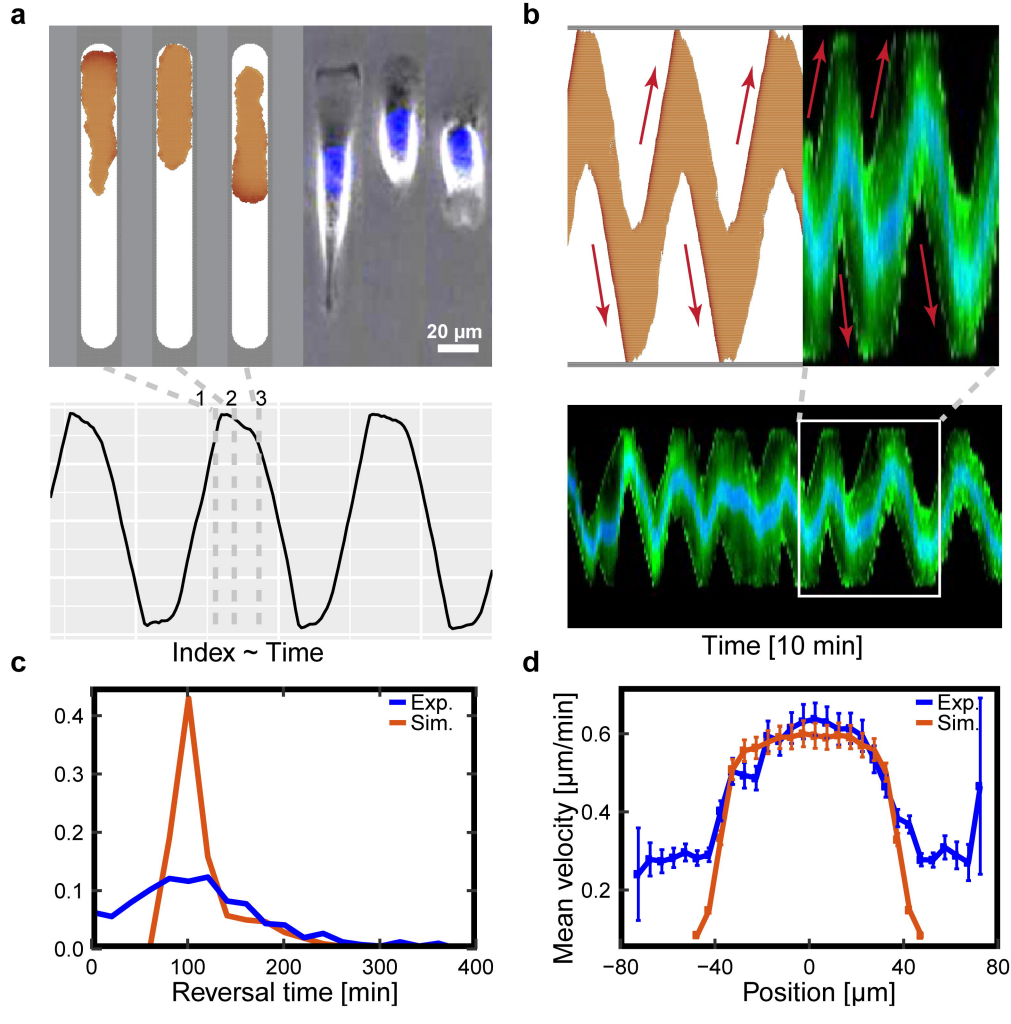
a
20 µm
1
2
3
Index ~ Time
b
Time [10 min]
c
Exp.
Sim.
0.4
0.3
0.2
0.1
0.0
0
100
200
300
400
Reversal time [min]
d
Exp.
Sim.
Mean velocity [µm/min]
0.6
0.4
0.2
−80
−40
0
40
80
Position [µm]

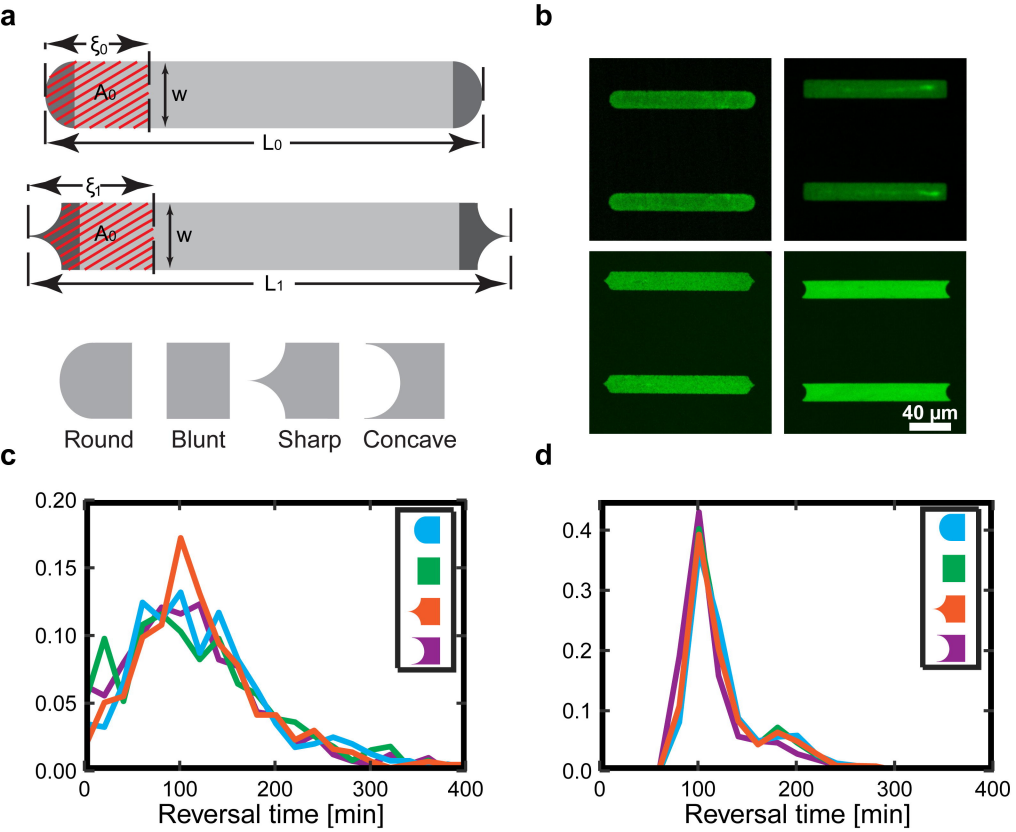
a
ξ0
A0
w
L0
ξ1
A0
w
L1
Round
Blunt
Sharp
Concave
b
40 μm
c
0.20
0.15
0.10
0.05
0.00
0
100
200
300
400
Reversal time [min]
d
0.4
0.3
0.2
0.1
0.0
0
100
200
300
400
Reversal time [min]

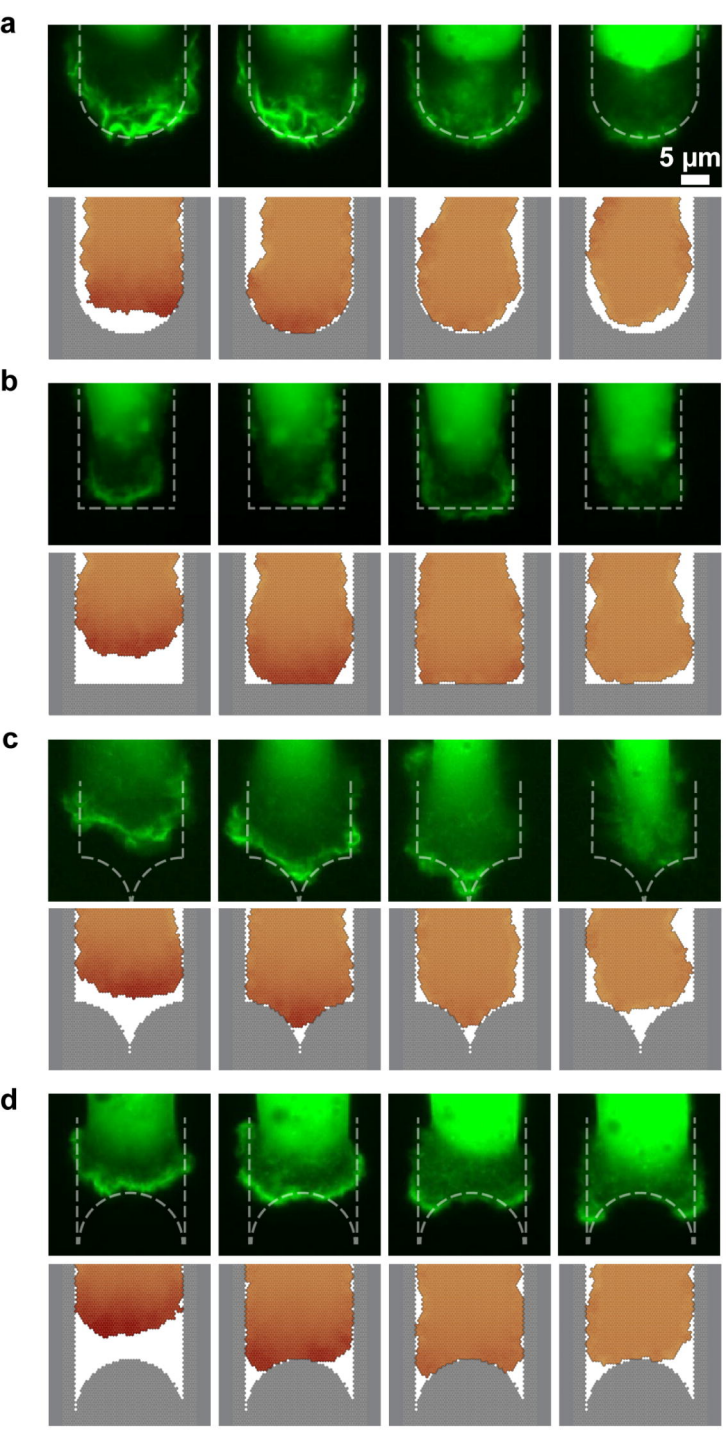
a
5 μm
b
c
d